Carbohydrate Polymer Technologies and Applications 8 (2024) 100574

Contents lists available at ScienceDirect

Carbohydrate Polymer Technologies and Applications

journal homepage: www.sciencedirect.com/journal/carbohydrate-polymer-technologies-and-applications

Enhancing emulsion stability and adsorption of Pickering emulsions using alkylated cellulose nanofibers

Miyu Tanzawa [a], Noriko Kanai [b], Takahiro Sakai [c], Kohei Yamada [a], Sari Kumagai [a], Batsaikhan Mijiddorj [d], Izuru Kawamura [a,*]

[a] Graduate School of Engineering Science, Yokohama National University, Yokohama, Kanagawa 240-8501, Japan
[b] Graduate School of Environment and Information Sciences, Yokohama National University, Yokohama, Kanagawa 240-8501, Japan
[c] R&D Center, T. Hasegawa Co., Ltd., 29-7 Kariyado, Nakahara, Kawasaki, Kanagawa, 211-0022, Japan
[d] Department of Biology, School of Arts and Sciences, National University of Mongolia, Ulaanbaatar 14201, Mongolia

ARTICLE INFO

Keywords:
Cellulose nanofibers
Pickering emulsion
Stability
Alkylated cellulose nanofibers
Hydrophobic modification

ABSTRACT

Cellulose nanofibers (CNFs) extracted from plant cell walls form a three-dimensional network in water and stabilize the dispersion of droplets, which are used as emulsion stabilizers. In this study, four types of alkyl-grafted CNFs (ACNFs) with different lengths of dialkyl chains (diC4, diC6, diC8, and diC10) were synthesized by the surface modification of 2,2,6,6-tetramethylpiperidine-1-oxyl radical (TEMPO)-oxidized CNF (TOCNF) to improve the stability of oil-in-water Pickering emulsions (PEs). The ACNF-stabilized emulsions with a 20/80 ratio of oil/water were prepared using two different oils (olive oil and eucalyptus oil) and the ACNF 1.0 % dispersion, and the changes over time were investigated at approximately 25 °C. Compared to TOCNF, the ACNFs provided more stable olive oil-PE (o-PE) and eucalyptus oil-PE (e-PE) although the stabilization behaviors of o-PE and e-PE differed. Olive oil, which contained rich long-chain fatty acids, was more likely to interact with the ACNFs, thereby promoting the interfacial adsorption of oil droplets. On the other hand, eucalyptus oil is mainly composed of 1,8-cineole and does not have alkyl chains, so the interaction with the ACNFs was weak and therefore, sufficient interfacial adsorption could not be obtained. The results of the particle size distribution and viscosity measurements also showed that the ACNFs contributed significantly to the stabilization of o-PE. Based on the overall experimental results, it was determined that the diC6-ACNF gave the most significant stability improvement. Therefore, we designed an alkylated CNF that mimics diC6-ACNF for MD simulations. MD simulations showed that hydrophobic modification created a hydrophobic interaction between the alkyl chain and dodecane molecules as the oil, leading to the enhancing adsorption of ACNF at the oil droplet interfaces.

1. Introduction

An emulsion is a mixture of two immiscible liquids, oil and water, stabilized by surfactants with amphiphilic properties. Instead of using molecular-based surfactants, which may cause environmental or health issues, Pickering emulsions (PEs), a system that uses nano- or micro-scale particles as stabilizers/emulsifiers, are of great interest to researchers because of their high stability, quality, functionality, and renewability (Chevalier & Bolzinger, 2013; Wu & Ma, 2016; Zhu et al., 2021). Natural biopolymers such as proteins (Ding et al., 2019), starch (Wang et al., 2020), lignin (Dai et al. 2019), nanocelluloses (Fujisawa et al., 2017) have attracted global attention owing to the growing demand of replacing synthetic emulsifiers to renewable ones (Costa et al., 2019).

Nanocelluloses, isolated from a broad range of plant-based biomasses through chemical and/or mechanical nanofibrillation, have been extensively studied as promising stabilizers for PEs. The most common types of nanocelluloses, cellulose nanocrystals (CNCs) and cellulose nanofibers (CNFs), are characterized by their aspect ratio. Short and low aspect-ratio CNCs align side by side on the droplet surface, achieving high coverage whereas long, high aspect-ratio CNFs form a strong interconnected droplet network preventing coalescence (Kalashnikova et al., 2013; Lu et al., 2021). The stability of nanocellulose-stabilized PEs is affected by the overall balance of nanocellulose (e.g., aspect ratio and surface charge), oil types (polarity and viscosity), and other diverse factors (e.g., temperature and pH).

* Corresponding author.
E-mail address: kawamura-izuru-wx@ynu.ac.jp (I. Kawamura).

https://doi.org/10.1016/j.carpta.2024.100574

Available online 25 September 2024

Pickering particles must have partial wettability in both oil and water phases for adsorption onto the interfaces (Aveyard et al., 2003). The (200)β/(220)α hydrophobic edge plane in nanocelluloses oriented toward the oil phase plays a critical role in dual wettability (Kalashnikova et al., 2012). The highly hydrophilic surface character of nanocelluloses stabilizes oil-in-water (o/w) PEs; however, its low hydrophobicity limits stabilization when natural oils that contain various compounds. The long-term stability of the PEs stabilized by 2,2,6,6-tetramethylpiperidine-1-oxyl radical (TEMPO)-oxidized CNFs (TOCNFs) was compared using two types of oils, dodecane (single oil) and olive oil (multi-component oil), and olive oil PEs was found to be less stable than dodecane PEs (Kanai et al., 2022). The olive oil droplets, with a mean diameter of 6–8 μm (o/w = 20:80), formed flocs induced by the attractive force derived from CNF concentration gradients around droplets. This led to significant coalescence and Ostwald ripening, resulting in the bimodal droplet size distributions (DSDs), which eventually caused separation within one month.

Hydrophobic modification of nanocellulose is a successful method for enhancing PE stabilization. Zhang et al. performed the carboxylation of CNCs using TEMPO-mediated oxidation and then introduced hydrophobic alkyl groups with different alkyl chain lengths of alkylamines (carbon number, C3-C7) via peptide coupling (Zhang et al., 2017). They reported that butyl-grafted CNCs reduced the interfacial tension between oil and water, resulting in smaller oil droplets with a diameter of 250 nm. In contrast, only a few μm were obtained using carboxylated CNCs. Moreover, the authors found that the ratio of grafted alkyl groups to residual COOH groups was an important parameter for determining the droplet size. Seo et al. used bacterial CNFs (BCNFs) grafted with three different lengths of a single alkyl chain (carbon number, C6, 12, 18) and obtained stable *n*-decane and olive oil o/w PEs over 7 days with C18-BCNFs grafted concentrations of 0.18–0.36 mmol/g (Seo et al., 2021). The C18-BCNFs were interconnected due to the strong hydrophobic interactions above 0.36 mmol/g, resulting in larger droplets. In addition, didecane chain-grafted BCNFs (diC10-BCNF) exhibited strong interfibrillar associations at the interface (Bae et al., 2022). To the best of our knowledge, there have been no investigations into the enhancement of emulsion stability and atomic-level interfacial interactions between oils and TOCNFs derived from agricultural waste grafted with various lengths of double alkyl chains. Molecular dynamics simulations were performed to investigate the difference in interaction with oil due to modified/unmodified alkyl chains and the compatibility with the results of emulsification experiments.

Natural oils are more desirable than petroleum-derived oils for PEs in food, cosmetic, and pharmaceutical applications (Albert et al., 2019). In the cosmetics industry, silicone oil (Wu et al., 2020), which is a petroleum-derived oil, and rice oil (Bernardi et al., 2011), which is a vegetable oil, have been studied for the oils of emulsions. For example, olive oil, one of the most traded vegetable oils, primarily consists of triglycerides (95–98 %) with ~80 % oleic acid (C18:1) followed by ~10 % palmitic acid (C16:0) and various minor components such as squalene and carotenoids (Chapagain & Wiesman, 2009; Stefanoudaki et al., 1999). Eucalyptus oil extracted from *Eucalyptus* leaves consists of ~80 % 1,8-cineol (also known as Eucalyptol) and is an important essential oil for cosmetic and pharmaceutical industries (Elaissi et al., 2012; Sebei et al., 2015).

In this study, to improve the stability of oil-in-water Pickering emulsions, four types of site-specific dialkyl chain grafted CNFs (ACNFs) were synthesized from waste hop stem-derived TOCNF and used as emulsifying stabilizers using olive oil and eucalyptus oil. Furthermore, the enhanced emulsion stability of the ACNFs was demonstrated through confocal laser scanning microscopy (CLSM) and particle size distribution measurements. Molecular dynamics (MD) simulations revealed atomic-level interactions between the double alkyl chains on the CNFs and oil droplets.

2. Experimental

2.1. Materials

Air-dried waste hop stems were mechanically milled and used as raw materials for CNFs. Hop stems air-dried for more than a year were provided by Tono Ryokuho High School, Japan, and used as raw materials for CNFs. The hop stems were mechanically milled into fine particles using a dry-defibrating machine (West Japan Engineering, Inc.). 2,2,6,6-tetramethylpiperidine-1-oxyl radical (TEMPO, 98 %), sodium bromide (NaBr, >99.0 %), sodium hypochlorite solution (NaClO, +5.0 %), HCl, NaOH were used for TEMPO oxidation. Congo Red and Nile Red were used for the dyes. Olive oil (0.909–0.915 g/mL) and eucalyptus oil (0.905–0.925 g/mL) were used for the oils. N-hydroxysuccinimide (NHS, 98.0 %) and N-(3-Dimethylaminopropyl)-N'-ethylcarbodiimide hydrochloride (EDC, 92+%) were used for synthetic reagents. Dibutylamine, dihexylamine, diocthylamine, and didecylamine were used for hydrophobic modification. All chemicals were purchased from Wako Pure Chemical (Japan).

2.2. Hydrophobic modification of TOCNFs using dialkylamine

TOCNFs (1 wt%) were isolated from waste hop stems according to the previous study (Kanai et al., 2022). The median width of the TOCNFs was 1.7 ± 0.7 nm and the carboxylate content determined from the electric conductivity titration was 0.84 mmol g^{-1}. Alkyl-grafted CNFs (ACNFs) were prepared according to a modified version of the method of Seo et al. (2021). EDC (0.3 mmol) and NHS (1.1 mmol) were added to a 1 wt% TOCNF dispersion (40 g) and stirred for 15 min at room temperature to activate the carboxyl groups. Dialkylamine (0.6 mmol) with four different alkyl chain lengths, dibutylamine (diC4), dihexylamine (diC6), diocthylamine (diC8), and didecylamine (diC10) was dissolved in ethanol (10 mL) and added to the activated 1 wt% TOCNF dispersion (Fig. 1**a**). The mixture was stirred at 50 °C overnight and then, dialysis was performed for 3 days followed by centrifugation at 5000 rpm for 2 h to collect the slurry. The slurry was dispersed in distilled water at 1 wt% using a homogenizer (BRANSON, Sonifer SEF250) for 1.5 min in the pulse mode with a 1/4″ microtip at an amplitude setting of 40 % to obtain ACNFs. ACNFs with four different alkyl chain lengths were named diC4-ACNF, diC6-ACNF, diC8-ACNF, diC10-ACNFs.

2.3. Emulsification

Olive oil or eucalyptus oil was added to the 1 % TOCNFs or ACNFs dispersions with oil/water ratios of 20/80 by weight and the mixture (approximately 25 g) was pre-stirred by vortex mixer. The o/w PEs were prepared using the homogenizer for 1 min at 40 % amplitude (Fig. 1**b**). The TOCNFs or ACNFs-stabilized olive oil Pickering emulsions (o-PEs) and eucalyptus oil Pickering emulsions (e-PEs) were stored at approximately 25 °C for one month. The PE samples were characterized on day 1, one week later (day 7), and approximately one month (days 28–31) after emulsification.

2.4. Solid-state nuclear magnetic resonance

The freeze-dried TOCNFs or ACNFs were directly packed into a zirconia NMR rotor with an outer diameter of 4.0 mm. ^{13}C Cross-polarization magic angle spinning (CP-MAS) NMR experiments were carried out using a 600 MHz NMR spectrometer (Bruker Avance III) equipped with a 4.0 mm $^{1}H/^{13}C/^{15}N$ triple-resonance E-free MAS probe at 298 K with a contact time of 1–1.5 ms and a recycle delay time of 3 s under a MAS frequency of 12.5 kHz.

2.5. Confocal laser scanning microscopy

The o-PEs and e-PEs were stained using 5 μL of Congo red (1 mg/mL)

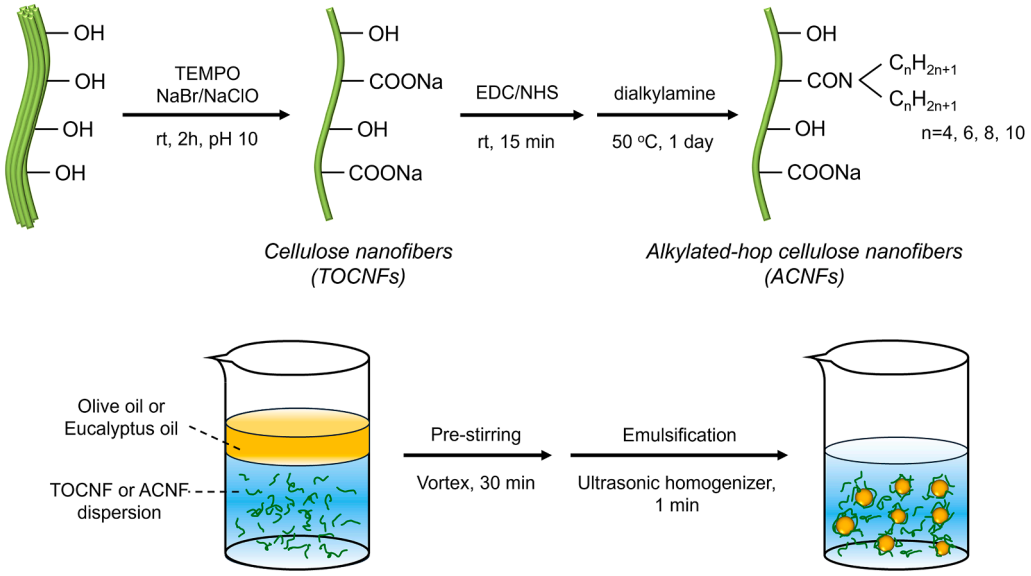

Fig. 1. (a) Reaction scheme of hydrophobic surface-modification with dialkylamine on the TOCNFs. (b) Schematic diagram of emulsification with oil droplets (yellow) in the water phase (blue) stabilized by TOCNF or ACNF (green).

or Nile red (1 mg/mL-ethanol) to visualize the CNFs or oils, respectively. The straining solution was added to freshly prepared PEs (0.5 g) and mixed by vortex mixer. CLSM images were acquired using a Carl Zeiss LSM5 using a × 63 oil-immersion DIC objective lens controlled by ZEN2009 software. Two to five CLSM images were acquired from different locations. The fluorescence of Congo red-stained PEs was excited with Ar 488 nm/HeNe 534 nm lines and detected using a 560 nm long-pass filter for emission, whereas Nile red-stained PEs were excited with Ar 488 nm lines and detected using 505–530 nm band-pass filter for emission.

2.6. Rheological measurement

The viscosities of the o-PEs and e-PEs were characterized using a rotational rheometer, (RheolabQC, Anton Paar) with a temperature control unit (C-PTD 180) and a concentric cylinder measuring system (CC-27). The data were collected at 25 °C between the shear rate range of 0.1–100 s^{-1} using a logarithmic ramp with 50 points obtained every 5 s duration. Viscosity measurements taken for round-trip were repeated twice.

2.7. Droplet size distribution

The DSDs of o-PEs and e-PEs were investigated on days 1, 7, 29, and 30 using a laser scattering particle size distribution analyzer (LA-950V2, HORIBA) in wet mode. A drop of PE was added to the water medium until the light transmittance of the red laser and blue LED reached 90–80 % and 90–70 %, respectively, after which the samples were sonicated to remove air bubbles and stirred at 2000 rpm. The DSDs were determined on a volume basis within the range of 0.01–2000 μm. The measurements were performed two or three times.

2.8. MD simulation

The initial system containing a single unmodified CNF was prepared using the CHARMM-GUI glycan reader and modeler (Jo et al., 2008; Park et al., 2019), which was adjusted for use with AMBER (Tian et al., 2020) and GLYCAM06j force fields (Kirschner et al., 2008). The CNF consisted of 18 chains, each comprising 20 d-glucose units. Twenty residues on the CNF surface were carboxylated and alkylated glucose residues at similar positions (Fig. S1). The partial charges of these altered residues were calculated using GAUSSIAN09 version A02 (Frisch et al., 2009), employing the B3LYP/6-31++G(2d,2p) theory level according to the GLYCAM06j force field. The restrained electro static potential (RESP) method was used for the calculations (Bayly et al., 1993). The parameters of the altered residues were generated using the antechamber module of the AmberTools23 package (Case et al., 2023), and the dihedral angle parameters around the modified regions were appended using the General Amber Forcefield for carboxylated and alkylated residues (Wang et al., 2004). Subsequently, the topologies of CNF's modified chains were created using AmberTools23 and then transformed into the GROMACS format using the ACPYPE software (Bernardi et al., 2019). Detailed information regarding the simulation system is presented in Table 1.

MD simulations were performed using GROMACS 2021.6 (Van Der Spoel et al., 2005) with the explicit inclusion of a solvent (TIP3P) under isothermal–isobaric (NPT) conditions (Jorgensen & Jenson, 1998; Jorgensen et al., 1983). Standard minimization, equilibration, and production setups of the CHARMM-GUI glycan reader and modeler were applied to all simulations (Park et al., 2019). The systems were energy-minimized (steepest descent) and equilibrated in the NPT ensemble for 500 ps with 0.001 ps time steps. In the MD simulations, isotropical Parrinello-Rahman barostat maintained the pressure at 1 bar with $\tau_P = 5.0$ ps and compressibility of 4.5×10^{-5} bar^{-1} (Parrinello & Rahman, 1981). The temperature of the Nose-Hoover thermostat was maintained at 303.15 K (Evans & Holian, 1985; Hoover, 1985; Nosé, 1984). The Particle Mesh Ewald (PME) method was employed to calculate long-range electrostatic interactions with a real-space cutoff distance of 0.9 ns (Darden et al., 1993). The Verlet cutoff scheme was

Table 1
Information of simulation systems.

Systems	CNF	Water	Dodecane	Na	Cl	Time, ns (# of simulations)
Car. CNF in water	1	51,887	0	176	156	100
Alk. CNF in water	1	52,219	0	148	148	100
Car. CNF in water and oil	1	48,786	400	176	156	100 (x3)
Alk. CNF in water and oil	1	48,488	400	148	148	100 (x3)

employed for neighbor searching within a 0.9 nm distance (Bussi et al., 2007). The Van der Waals interactions were set at a cutoff distance of 0.9 nm. The bond lengths involving hydrogen atoms were fixed using the LINCS algorithm (Hess et al., 1997). Trajectories were saved at 100 ps intervals for analysis. Visual Molecular Dynamics (VMD) was used for molecular visualization (Humphrey et al., 1996).

3. Results and discussion

3.1. Solid-state NMR characterization of the TOCNF and alkyl-grafted CNFs

The reaction scheme for the hydrophobic surface-modification with dialkylamine on the TEMPO-oxidized CNFs is shown in Fig. 1**a**. In this reaction, the C6 carboxyl groups were activated by EDC/NHS, and then dialkyl chains were grafted by forming amide bonds. ^{13}C CP-MAS NMR spectra of the four types of dried ACNFs (diC4, diC6, diC8, and diC10-ACNFs) along with the TOCNFs are shown in Fig. 2. There was no substantial change in the shape of the glucose unit peaks (60–110 ppm) between the TOCNFs and ACNFs, indicating that surface modification did not significantly affect the cellulose structures. The peaks at around 10–50 ppm were assigned to the alkyl chains of the ACNFs. Note that the peak at 30–35 ppm in the TOCNFs is possibly due to residual other lipids. The ^{13}C NMR signals of the alkyl group were assigned according to the literature (Buffy et al., 2003). In the NMR spectrum of dried diC4, the signals of methyl carbons (-$\underline{C}H_3$) in the di-butyl chain were observed split at 13.8 ppm and 15.0 ppm. Additionally, the broad ^{13}C NMR signals of methylene carbon α (-$C_\beta H_2$-$\underline{C\alpha}H_2$-CH_3), methylene carbon β (-$\underline{C\beta}H_2$-$C_\alpha H_2$-CH_3), and -N-$\underline{C}H_2$-$C_\beta H_2$-$C_\alpha H_2$-CH_3 were observed at 20, 30, 44 ppm, respectively. This suggests that the hydrocarbon chains were too short, preventing interactions between the butyl chains in diC4 and resulting in a conformationally inhomogeneous state. The NMR pattern of six signals of diC6 was similar to that of diC4 and slightly broader in linewidth. In the case of diC8, the relatively sharp signals of the methyl carbons were observed at 14.1 ppm, with the sharp signals of methylene carbon α (-$C_\beta H_2$-$\underline{C\alpha}H_2$-CH_3) at 22.7 ppm, methylene carbon β (-$\underline{C\beta}H_2$-$C_\alpha H_2$-CH_3) at 32 ppm, methylene carbons γ, δ, φ (-$\underline{C\varphi}H_2$-$C_\varepsilon H_2$-$\underline{C\delta}H_2$-$\underline{C\gamma}H_2$-$C_\beta H_2$-$C_\alpha H_2$-CH_3) at 29.3 ppm, methylene carbon ε (-$C_\varphi H_2$-$\underline{C\varepsilon}H_2$-$C_\delta H_2$-$C_\gamma H_2$-$C_\beta H_2$-$C_\alpha H_2$-$CH_3$) at 27.5 ppm, and -N-$\underline{C}H_2$- at 47 ppm. Spectral identification of diC10 was similar to that of

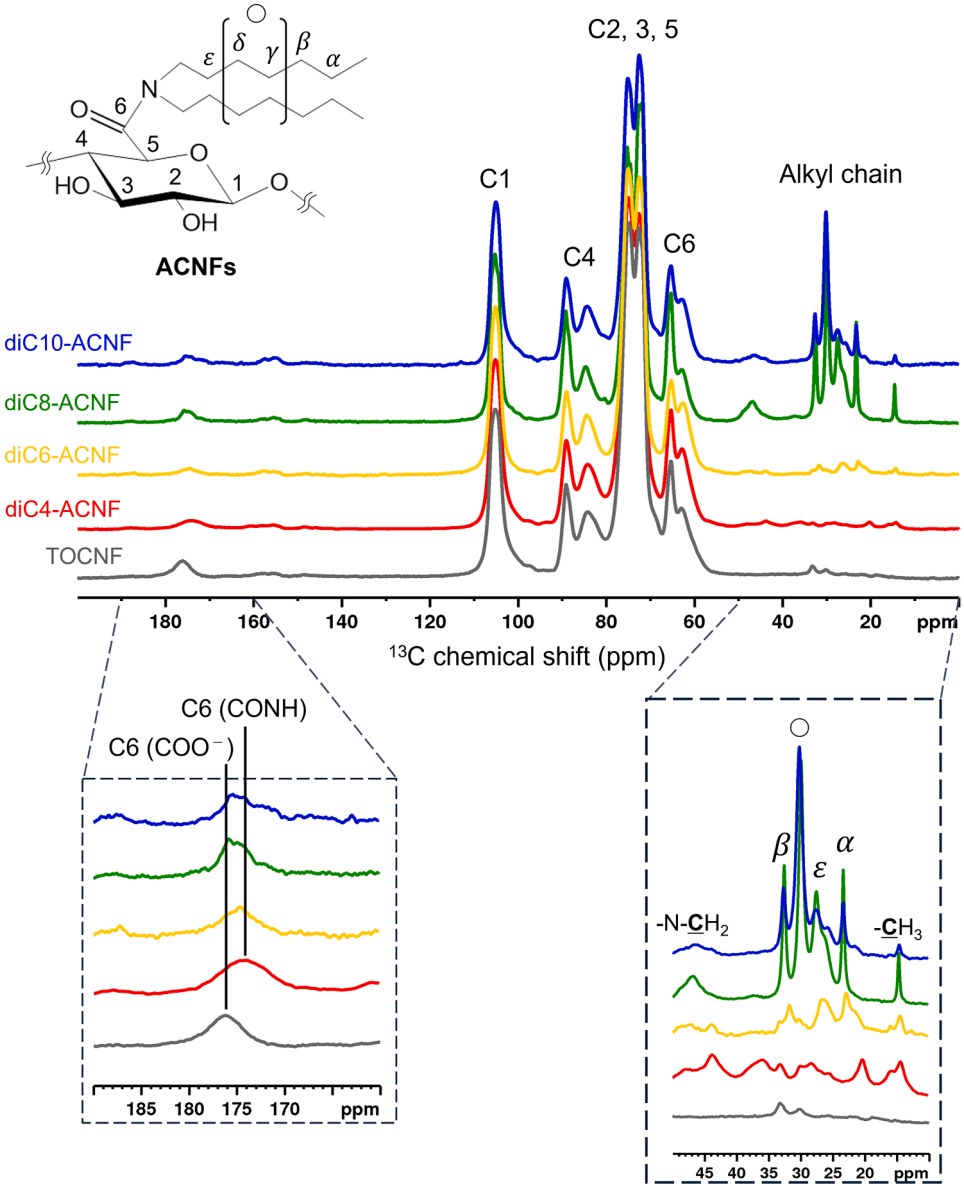

Fig. 2. ^{13}C CP-MAS solid-state NMR spectra of TOCNFs and ACNFs. CεH_2 is present only in diC6, diC8, and diC10-ACNF.

diC8. This suggests that the conformation of the alkyl groups in diC8 and diC10 was homogenous, even in the dried state. The broad peak observed at 176 ppm was attributed to the carboxyl group at the C6 position, which was converted via TEMPO-mediated oxidation. This peak was slightly shifted to a lower ppm (174 ppm) for all ACNFs, which was attributed to the amide carbonyl derived from the amide bond generated by surface modification. Consequently, the signal assignments of the alkyl groups for all ACNFs were archived, confirming the surface modification of the TOCNFs with di-alkyl groups. The carboxyl content of the TOCNFs obtained using the electric conductivity titration method was 0.838 mmol/g, whereas those of the diC4, diC6, diC8, and diC10-ACNFs were 0.588, 0.677, 0.680, and 0.564 mmol/g, respectively (Fig. S2). The corresponding modification rates calculated from these results were 4.06, 2.61, 2.56, and 4.44 %, respectively.

3.2. *Alkyl-grafted CNFs-stabilized Pickering emulsion*

The time courses of the CLSM images of o-PEs and e-PEs stabilized by TOCNFs or ACNFs are shown in Figs. 3 and 4. The TOCNFs and ACNFs were stained with Congo red (Figs. 3**a** and 4**a**), whereas the olive and eucalyptus oil were stained with Nile red (Figs. 3**b** and 4**b**). For TOCNF-stabilized o-PEs, destabilization mechanisms such as coalescence and Ostwald ripening of olive oil droplets promptly progressed from the day after emulsification, resulting in larger oil droplets (Fig. 3**a**). In addition, the oil droplets aggregated to form flocs (Fig. 3**b**). The CNF network-stained red was formed in the continuous phase; however, the oil droplet interfaces were not strongly stained, indicating that only a small amount of TOCNFs were adsorbed on the interfaces.

In contrast, strong staining of the ACNFs at the oil droplet interface was observed, indicating that more ACNFs were adsorbed by the surface modification of the dialkyl chain. The oil droplet coated with the ACNFs were smaller than those coated with the TOCNFs and were isolated for 30 days. In particular, the diC6- and diC8-ACNFs emulsions showed stable adsorption throughout the storage period. This can be explained by the hydrophobic interactions between the modified alkyl chains and the oil droplets. The alkyl chain on the ACNFs acts as an anchor into oil droplets, allowing the ACNFs to cover the oil droplet surfaces, resulting in a lower interfacial energy.

The DSD and growth speed over time were different in e-PEs compared to o-PEs. With o-PE, there was no noticeable coalescence of oil droplets throughout the 30 days; however, with e-PE, the oil droplet size increased after 7 days, indicating that coalescence progressed more quickly. Because no staining was observed at the oil droplet interface, it is thought that the droplet size significantly increased over time (Fig. 4**a**). The diC4-ACNFs did not improve the ACNF adsorption, indicating that the diC4 chain length was not long enough to obtain sufficient hydrophobic interaction with the eucalyptus oil droplets.

In addition, the differences in the oil components may have affected the instability behavior between the o-PEs and e-PEs. Olive oil consists of long-chain triglycerides with ~80 % monounsaturated fatty acids and ~10 % saturated acids and various polar minor components, whereas eucalyptus oil is an essential oil, mainly consists of 1,8-cineole and other minor components such as α-pinene and trans-pinocarveol (Sebei et al., 2015). The long-chain hydrocarbons in the olive oil could have enhanced the hydrophobic interactions with dialkylamines, leading to higher stability of the ACNF-stabilized o-PEs.

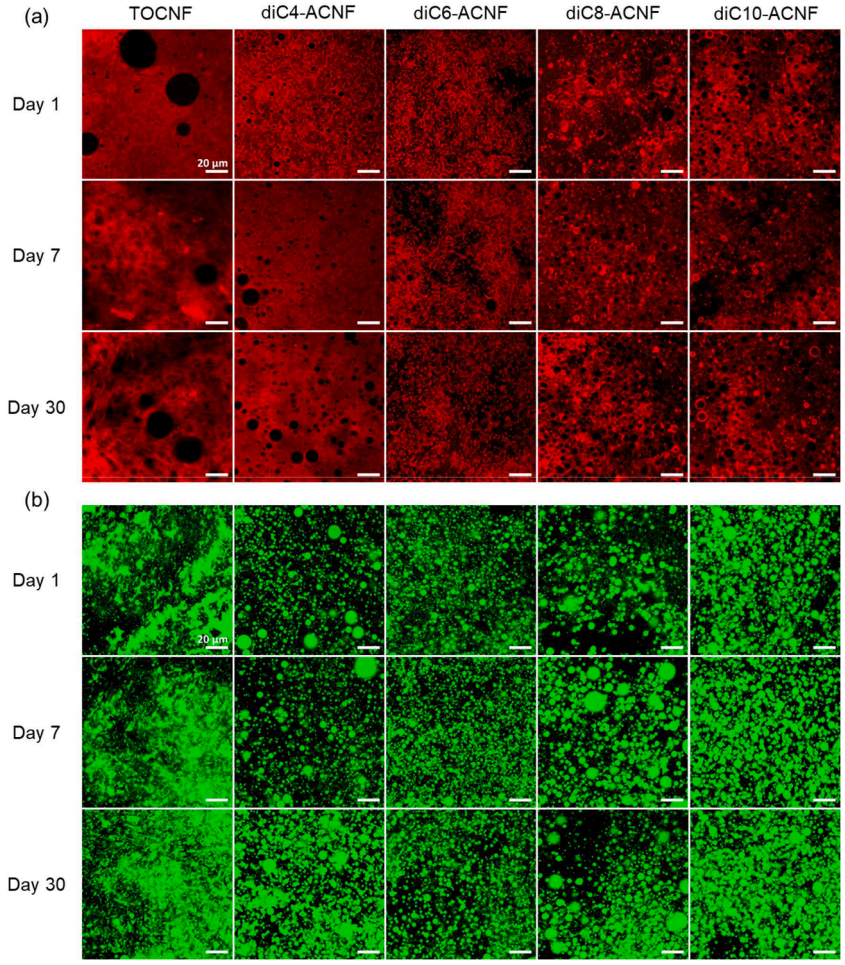

Fig. 3. CLSM images of o-PEs stained (a) TOCNFs or ACNFs with Congo red and (b) olive oil with Nile red. The scale bar represents 20 μm.

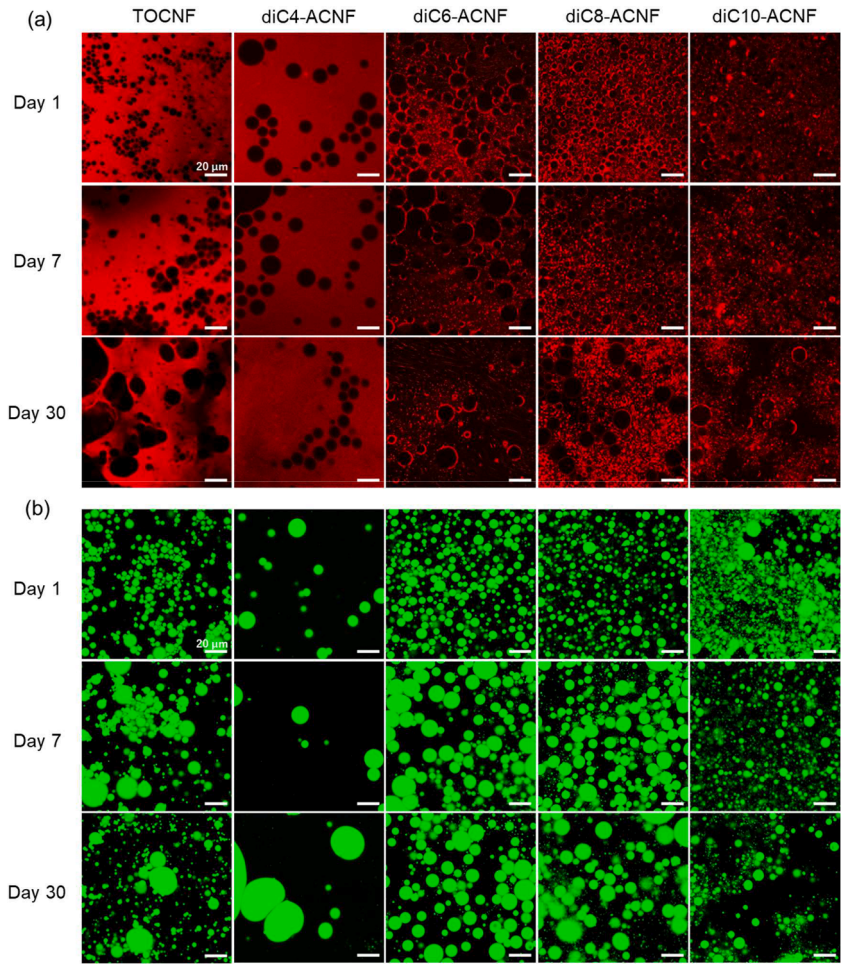

Fig. 4. CLSM images of e-PEs stained (a) TOCNFs or ACNFs with Congo red and (b) olive oil with Nile red. The scale bar represents 20 μm.

3.3. Droplet size distributions

The DSD of the o-PEs and e-PEs are shown in Fig. 5. Even for the same ACNFs, significant differences in the distribution widths were observed depending on the type of oil. While the DSD of the TOCNFs for o-PEs was bimodal having two different modes at around 2–4 μm and 100 μm, the ACNFs were monomodal, having <10 μm modes. The average diameter of the diC4-, diC6-, diC8-, and diC10-ACNFs on day 1 were 3.09, 3.28, 8.91, and 3.24 μm, respectively, and these values remained almost for a month. Initially, small diameters were more frequent; however, over time, the shoulder peak of the distribution broadened. This is attributed to the growth of the oil droplets.

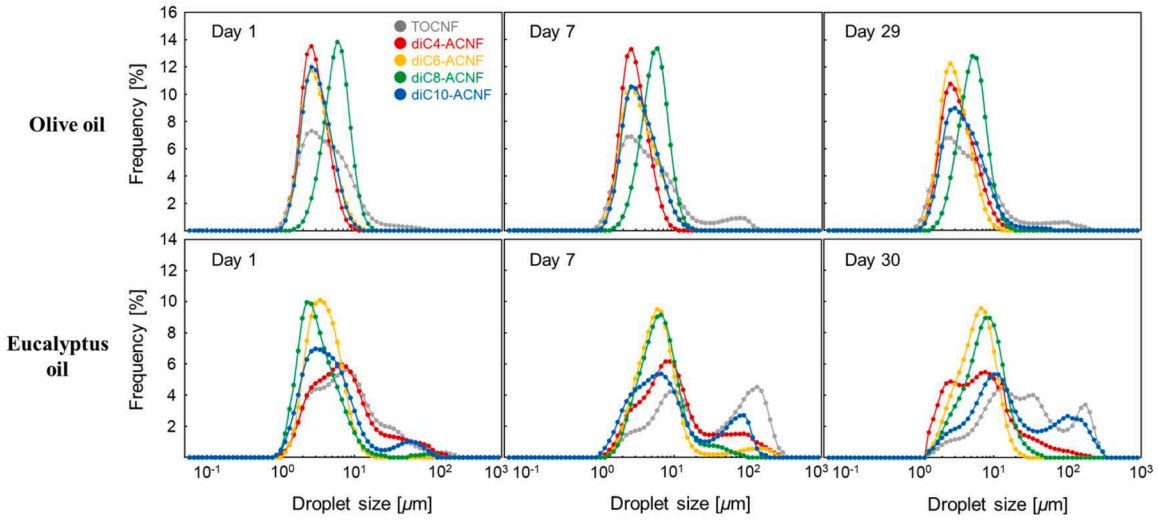

Fig. 5. Droplet size distributions of o-PEs and e-PEs stabilized by TOCNFs (grey), diC4- (red), diC6- (orange), diC8- (green), and diC10-ACNFs (blue) on days 1, 7, and 29/30.

In contrast, the DSD of the e-PEs showed significant differences among the four ACNFs. The distribution shapes of the diC4- and diC10-ACNFs were similar to those TOCNF, showing multimodal distributions since day 1. After 30 days, not only did the distribution expand, but oil droplets of various sizes were also observed, which is thought to be the cause of the instability. For the diC6- and diC8-ACNFs, droplets larger than 100 μm were scarce, and their distribution widths were sharper. Coalescence is thought to be the main reason for the increase in droplet size; however, considering the DSD results for o-PEs and e-PEs, it can be said that diC6 and diC8-ACNFs prevented coalescence between oil droplets.

3.4. Rheological measurements

The apparent viscosities of Pickering emulsions were investigated on days 1, 7, 29 and 30, and the downward curves are shown in Fig. 6. The viscosity decreased as the shear rate increased for all the emulsions, confirming that the thixotropic properties of the TOCNF were maintained. The ACNF-stabilized o-PEs had a higher viscosity than the TOCNF after 30 days. It was assumed that the low viscosity of diC8-ACNF was due to the lot differences. The low viscosity of diC8-ACNF is thought to be due to lot differences, but it increased over time, and on day 30, the viscosity at a shear rate of 0.1 s^{-1} exceeded 10 Pa s. The e-PEs exhibited lower viscosities than the o-PEs from day 1, regardless of the type of ACNFs. Because of its low viscosity, the values were scattered at low shear rates, making accurate measurements impossible. However, on day 30, the viscosity recovered and increased to the same level as that of o-PEs.

3.5. Molecular dynamics simulation

The absorption of alkylated and carboxylated CNFs in oil was investigated using MD simulations. Initially, we adapted each cellulose molecule in water during 100 ns of the simulations. Initial and final snapshots of the carboxylated and alkylated CNFs corresponding to the TOCNF and diC6-ACNF systems are shown in Fig. S1. Both CNF molecules exhibited a twisted structure throughout the simulations, which was consistent with previous observations of twisted cellulose nanofibers using both experimental and computational techniques (Bu et al., 2015; Conley et al., 2016; Fujisawa et al., 2023; Kannam et al., 2017; Khandelwal & Windle, 2014; Paavilainen et al., 2011). We then applied the structures of the CNF molecules in the last snapshot to the initial conformations of the subsequent simulations, in which dodecane molecules were arbitrarily inserted into the system to observe the interaction of the CNF molecules with the oil. Three independent 100 ns periods were conducted for both carboxylated and alkylated CNF in a mixture of oil and water.

We analyzed the interaction energy between both carboxylated and alkylated CNFs and dodecane molecules and found that the Lennard-Jones interaction term predominantly contributed to the interactions, compared to the Coulombic interaction. Fig. 7**a** shows the average Lennard-Jones interaction energies between the CNFs and dodecane molecules as a function of time. The alkylated CNF interacted more strongly with dodecane molecules (red line) than the carboxylated CNF (black line) during all three simulations. It indicates that the alkylated residue of CNF significantly enhances the interaction between CNF and oil molecules, suggesting that surface modification effectively increases

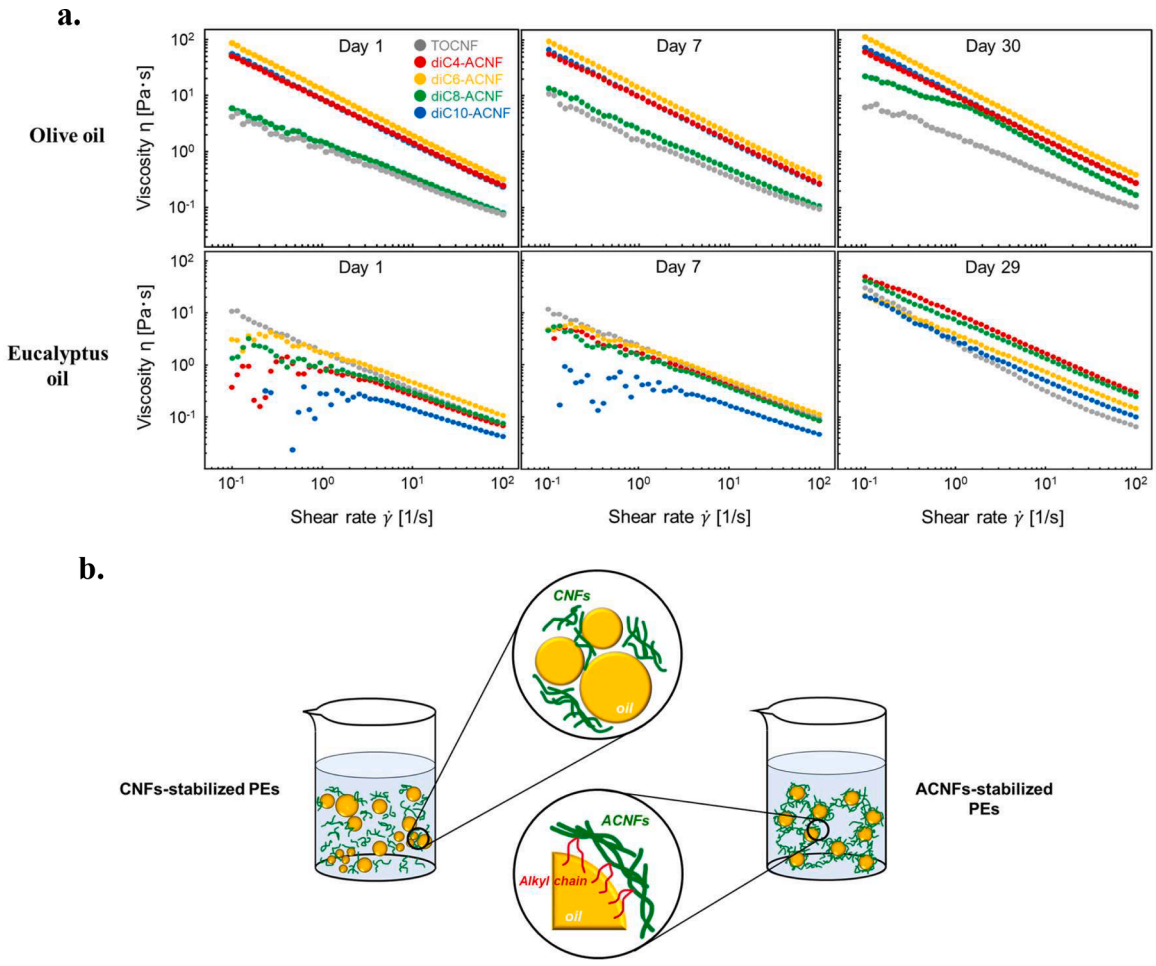

Fig. 6. (a) Viscosity of o-PEs and e-PEs stabilized by TOCNFs (grey), diC4- (red), diC6- (orange), diC8- (green), and diC10-ACNFs (blue) on days 1, 7, and 29/30. (b) Schematic diagram of CNFs (green) and ACNFs (green and red) and oil (orange) droplets in an emulsion (blue).

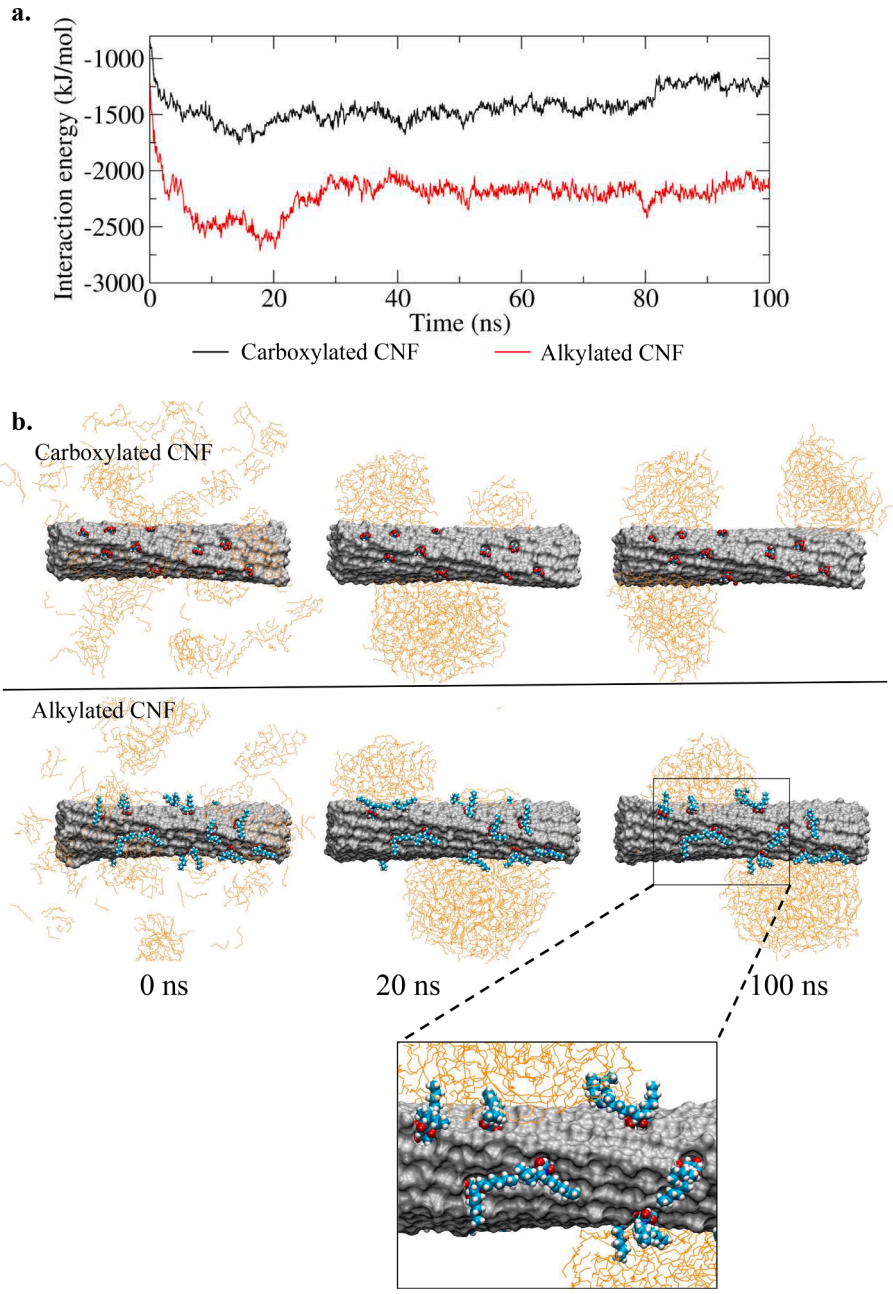

Fig. 7. (a) Averaged Lennard-Jones interaction energies of both carboxylated and alkylated CNFs with dodecane molecules as a function of time in the simulations. Three independent simulations of both systems were averaged and plotted for clarity. Black and red lines show the average interaction energies of carboxylated and alkylated CNF molecules, respectively, interacting with dodecane as a function of time. (b) Snapshots of carboxylated and alkylated CNFs interacting with dodecane molecules extracted from MD simulations, representing configurations closest to average interaction energies plot. Upper and lower panels show the snapshots of carboxylated and alkylated CNF interacting with dodecane molecules at 0, 20, and 100 ns, respectively. The final snapshot of alkylated CNF system, with an inset highlighting how the alkylated residues anchor to the oil surface. The CNF molecules are displayed with grey surfaces, and the dodecane molecules are shown in orange lines without protons for clarity. The carboxylated and alkylated glucose residues are represented using van der Waals (VDW) spheres representation. Water and ions were omitted for clarity. Structural figures were created using VMD software.

the hydrophobic interaction between CNF and oil.

Thus, we selected one simulation of carboxylated and alkylated CNFs interacting with dodecane molecules that were closer to the average interaction energy over time. We extracted snapshots of the carboxylated and alkylated CNFs interacting with dodecane molecules at 0, 20, and 100 ns from these trajectories shown in Fig. 7**b**. In all the simulations, randomly dispersed dodecane molecules aggregated into a drop-like shape around the hydrophobic surface of the CNFs (200 plane), as shown in Fig. 7**b**. This result agrees with the previously observed favourable interaction between oil and the hydrophobic face of the CNF crystal (Li et al., 2017). Interestingly, the alkylated residues close to the hydrophobic face of the CNF anchored into the oil drop during the simulations of the alkylated CNF. The anchoring role is shown in the inset of Fig. 7**b**. This specific anchoring role can also be extended to alkylated CNFs of different lengths. Further, our MD simulation results are suggested that multi-point interactions via multiple di-alkyl chains per ACNF molecule increase the total affinity interaction energy between an oil droplet and ACNF. The MD simulation results support the idea that introducing di-alkylated modifications on the CNF surface significantly enhances the attraction or favourable interactions between CNF and oil because of the anchoring of the residues to the oil surface.

4. Conclusions

In this study, TEMPO-oxidized CNF was modified with hydrophobic double alkyl chains to enhance its hydrophobicity to improve its amphiphilicity as an emulsifier for natural oils. The CLSM images revealed that the alkyl chains of ACNF hydrophobically interacted with the oil droplets, and more interfaces were covered with ACNF than with TOCNF, preventing oil droplets coalescence. The droplet size distribution of o-PE stabilized by TOCNF was bimodal, including the droplet sizes larger than 100 μm, while that of diC6-ACNF was monomodal, with a smaller average droplet size of 3 μm. The results of droplet size distribution and viscosity measurements indicated that the stability of e-PE was lower than that of o-PE, indicating that the oil properties influenced the hydrophobic interaction. The optimal modified alkyl chain length was difficult to predict before the emulsification experiments since the emulsion stability depended on the structure and other properties such as the main components of the oil and the strength of hydrophobic interactions. Calculations using MD simulations also showed that the hydrophobic surfaces of the ACNF with alkyl chains interacted favorably with the oil using the model oil, confirming the effect of alkylation on the oil droplets. It should be noted, however, the simulations using mixed oil such as the olive oil and eucalyptus oil used in this study were challenging and did not fully reproduce the actual system. In summary, TOCNF initially lacked long-term stability in highly hydrophobic oils such as vegetable oil, but alkyl chain modification strengthened the amphiphilicity and the stability was improved by promoting ACNF adsorption at the oil-water interface.

Funding

This work was supported in part by JSPS KAKENHI Grant Number (JP22KJ1398 and JP24K23119 to N.K., JP21H05229 to I.K.) and JST COI-NEXT program (JPMJPF2111 to I.K.).

CRediT authorship contribution statement

Miyu Tanzawa: Writing – original draft, Validation, Investigation, Formal analysis, Data curation. **Noriko Kanai:** Writing – original draft, Project administration, Investigation, Funding acquisition, Formal analysis, Data curation. **Takahiro Sakai:** Writing – review & editing, Validation, Investigation, Formal analysis. **Kohei Yamada:** Writing – review & editing, Validation, Investigation, Formal analysis. **Sari Kumagai:** Writing – review & editing, Validation, Investigation, Formal analysis. **Batsaikhan Mijiddorj:** Writing – review & editing, Validation, Investigation, Formal analysis. **Izuru Kawamura:** Writing – review & editing, Supervision, Funding acquisition, Formal analysis.

Declaration of competing interest

The authors declare that they have no known competing financial interests or personal relationships that could have appeared to influence the work reported in this paper.

Data availability

Data will be made available on request.

Acknowledgments

The authors acknowledge Dr. Yoichiro Tanaka and Mr. Shinji Ishihara of the Instrumental Analysis Center, Yokohama National University, for technical assistance with CLSM and solid-state NMR.

Supplementary materials

Supplementary material associated with this article can be found, in the online version, at doi:10.1016/j.carpta.2024.100574.

References

Albert, C., Beladjine, M., Tsapis, N., Fattal, E., Agnely, F., & Huang, N. (2019). Pickering emulsions: Preparation processes, key parameters governing their properties and potential for pharmaceutical applications. *Journal of Controlled Release: Official Journal of the Controlled Release Society, 309*, 302–332.

Aveyard, R., Binks, B. P., & Clint, J. H. (2003). Emulsions stabilised solely by colloidal particles. *Advances in Colloid and Interface Science, 100–102*, 503–546.

Bae, J., Seo, H. M., Shin, K., Choi, J., Lee, D. R., Jiang, Z., Shen, D., & Kim, J. W. (2022). Hydrophobically modified cellulose nanofibers-enveloped solid lipid microparticles for imporved antioxidant cargo retention. *Macromolecular Rapid Communications, 43*, Article 2100917.

Bayly, C. I., Cieplak, P., Cornell, W., & Kollman, P. A. (1993). A well-behaved electrostatic potential based method using charge restraints for deriving atomic charges: The RESP model. *The Journal of Physical Chemistry, 97*(40), 10269–10280.

Bernardi, A., Faller, R., Reith, D., & Kirschner, K. N. (2019). ACPYPE update for nonuniform 1–4 scale factors: Conversion of the GLYCAM06 force field from AMBER to GROMACS. *SoftwareX, 10*(100241), Article 100241.

Bernardi, D. S., Pereira, T. A., Maciel, N. R., Bortoloto, J., Viera, G. S., Oliveira, G. C., & Rocha-Filho, P. A. (2011). Formation and stability of oil-in-water nanoemulsions containing rice bran oil: In vitro and in vivo assessments. *Journal of Nanobiotechnology, 9*, 44.

Bu, L., Himmel, M. E., & Crowley, M. F. (2015). The molecular origins of twist in cellulose I-beta. *Carbohydrate Polymers, 125*, 146–152.

Buffy, J. J., Hong, T., Yamaguchi, S., Waring, A. J., Lehrer, R. I., & Hong, M. (2003). Solid-state NMR investigation of the depth of insertion of protegrin-1 in lipid bilayers using paramagnetic Mn^{2+}. *Biophysical Journal, 85*, 2363–2373.

Bussi, G., Donadio, D., & Parrinello, M. (2007). Canonical sampling through velocity rescaling. *The Journal of Chemical Physics, 126*(1), Article 014101.

Case, D. A., Aktulga, H. M., Belfon, K., Cerutti, D. S., Cisneros, G. A., Cruzeiro, V. W. D., Forouzesh, N., Giese, T. J., Götz, A. W., Gohlke, H., Izadi, S., Kasavajhala, K., Kaymak, M. C., King, E., Kurtzman, T., Lee, T.-S., Li, P., Liu, J., Luchko, T., … Merz, K. M., Jr (2023). AmberTools. *Journal of Chemical Information and Modeling, 63*(20), 6183–6191.

Chapagain, B. P., & Wiesman, Z. (2009). MALDI-TOF/MS fingerprinting of triacylglycerols (TAGs) in olive oils produced in the Israeli Negev desert. *Journal of Agricultural and Food Chemistry, 57*(4), 1135–1142.

Chevalier, Y., & Bolzinger, M. A. (2013). Emulsions stabilized with solid nanoparticles: Pickering emulsions. *Colloids and Surfaces. A, Physicochemical and Engineering Aspects, 439*, 23–34.

Conley, K., Godbout, L., Whitehead, M. A. T., & van de Ven, T. G. M. (2016). Origin of the twist of cellulosic materials. *Carbohydrate Polymers, 135*, 285–299.

Costa, C., Medronho, B., Filipe, A., Mira, I., Lindman, B., Edlund, H., & Norgren, M. (2019). Emulsion formation and stabilization by biomolecules: The leading role of cellulose. *Polymers, 11*(10), 1570.

Dai, L., Li, Y., Kong, F., Liu, K., Si, C., & Ni, Y. (2019). Lignin-based nanoparticles stabilized pickering emulsion for stability improvement and thermal-controlled release of trans-resveratrol. *ACS Sustainable Chemistry & Engineering, 7*(15), 13497–13504.

Darden, T., York, D., & Pedersen, L. (1993). Particle mesh Ewald: An N·log(N) method for Ewald sums in large systems. *The Journal of Chemical Physics, 98*(12), 10089–10092.

Ding, M., Zhang, T., Zhang, H., Tao, N., Wang, X., & Zhong, J. (2019). Effect of preparation factors and storage temperature on fish oil-loaded crosslinked gelatin nanoparticle pickering emulsions in liquid forms. *Food Hydrocolloids, 95*(April), 326–335.

Elaissi, A., Rouis, Z., Salem, N. A. B., Mabrouk, S., ben Salem, Y., Salah, K. B. H., Aouni, M., Farhat, F., Chemli, R., Harzallah-Skhiri, F., & Khouja, M. L. (2012). Chemical composition of 8 eucalyptus species' essential oils and the evaluation of their antibacterial, antifungal and antiviral activities. *BMC Complementary and Alternative Medicine, 12*, 81.

Evans, D. J., & Holian, B. L. (1985). The Nose–Hoover thermostat. *The Journal of Chemical Physics, 83*(8), 4069–4074.

Frisch, M. J., et al. (2009). *Gaussian 09, revision A.02, 34*. [Gaussian Inc: Wallingford CT].

Fujisawa, S., Daicho, K., Yurtsever, A., Fukuma, T., & Saito, T. (2023). Molecular dynamics of drying-induced structural transformations in a single nanocellulose. *Small (Weinheim an der Bergstrasse, Germany), 19*(30), Article e2302276.

Fujisawa, S., Togawa, E., & Kuroda, K. (2017). Nanocellulose-stabilized Pickering emulsions and their applications. *Science and Technology of Advanced Materials, 18*, 959–971.

Hess, B., Bekker, H., Berendsen, H. J. C., & Fraaije, J. G. E. M. (1997). LINCS: A linear constraint solver for molecular simulations. *Journal of Computational Chemistry, 18*(12), 1463–1472.

Hoover, W. G. (1985). Canonical dynamics: Equilibrium phase-space distributions. *Physical Review A: General Physics, 31*(3), 1695–1697.

Humphrey, W., Dalke, A., & Schulten, K. (1996). VMD: Visual molecular dynamics. *Journal of Molecular Graphics, 14*(1), 33–38, 27–28.

Jo, S., Kim, T., Iyer, V. G., & Im, W. (2008). CHARMM-GUI: A web-based graphical user interface for CHARMM. *Journal of Computational Chemistry, 29*(11), 1859–1865.

Jorgensen, W. L., Chandrasekhar, J., Madura, J. D., Impey, R. W., & Klein, M. L. (1983). Comparison of simple potential functions for simulating liquid water. *The Journal of Chemical Physics, 79*(2), 926–935.

Jorgensen, W. L., & Jenson, C. (1998). Temperature dependence of TIP3P, SPC, and TIP4P water from NPT Monte Carlo simulations: Seeking temperatures of maximum density. *Journal of Computational Chemistry, 19*(10), 1179–1186.

Kalashnikova, I., Bizot, H., Bertoncini, P., Cathala, B., & Capron, I. (2013). Cellulosic nanorods of various aspect ratios for oil in water Pickering emulsions. *Soft Matter, 9*(3), 952–959.

Kalashnikova, I., Bizot, H., Cathala, B., & Capron, I. (2012). Modulation of cellulose nanocrystals amphiphilic properties to stabilize oil/water interface. *Biomacromolecules, 13*(1), 267–275.

Kanai, N., Sakai, T., Yamada, K., Kumagai, S., & Kawamura, I. (2022). Using cellulose nanofibers isolated from waste hop stems to stabilize dodecane or olive oil-in-water Pickering emulsions. *Colloids and Surfaces. A: Physicochemical and Engineering Aspects, 653*, Article 129956.

Kannam, S. K., Oehme, D. P., Doblin, M. S., Gidley, M. J., Bacic, A., & Downton, M. T. (2017). Hydrogen bonds and twist in cellulose microfibrils. *Carbohydrate Polymers, 175*, 433–439.

Khandelwal, M., & Windle, A. (2014). Origin of chiral interactions in cellulose supramolecular microfibrils. *Carbohydrate Polymers, 106*, 128–131.

Kirschner, K. N., Yongye, A. B., Tschampel, S. M., González-Outeiriño, J., Daniels, C. R., Foley, B. L., & Woods, R. J. (2008). GLYCAM06: A generalizable biomolecular force field. Carbohydrates. *Journal of Computational Chemistry, 29*(4), 622–655.

Li, Y., Yu, S., Chen, P., Rojas, R., Hajian, A., & Berglund, L. (2017). Cellulose nanofibers enable paraffin encapsulation and the formation of stable thermal regulation nanocomposites. *Nano Energy, 34*(February), 541–548.

Lu, Y., Li, J., Ge, L., Xie, W., & Wu, D. (2021). Pickering emulsion stabilized with fibrous nanocelluloses: Insight into fiber flexibility-emulsifying capacity relations. *Carbohydrate Polymers, 255*, Article 117483.

Nosé, S. (1984). A molecular dynamics method for simulations in the canonical ensemble. *Molecular Physics, 52*(2), 255–268.

Paavilainen, S., Róg, T., & Vattulainen, I. (2011). Analysis of twisting of cellulose nanofibrils in atomistic molecular dynamics simulations. *The Journal of Physical Chemistry. B, 115*(14), 3747–3755.

Park, S.-J., Lee, J., Qi, Y., Kern, N. R., Lee, H. S., Jo, S., Joung, I., Joo, K., Lee, J., & Im, W. (2019). CHARMM-GUI Glycan Modeler for modeling and simulation of carbohydrates and glycoconjugates. *Glycobiology, 29*(4), 320–331.

Parrinello, M., & Rahman, A. (1981). Polymorphic transitions in single crystals: A new molecular dynamics method. *Journal of Applied Physics, 52*(12), 7182–7190.

Sebei, K., Sakouhi, F., Herchi, W., Khouja, M. L., & Boukhchina, S. (2015). Chemical composition and antibacterial activities of seven Eucalyptus species essential oils leaves. *Biological Research, 48*, 1–5.

Seo, H. M., Seo, M., Shin, K., Choi, S., & Kim, J. W. (2021). Bacterial cellulose nanofibrils-armored Pickering emulsions with limited influx of metal ions. *Carbohydrate Polymers, 258*(December 2020), Article 117730.

Stefanoudaki, E., Kotsifaki, F., & Koutsaftakis, A. (1999). Classification of virgin olive oils of the two major Cretan cultivars based on their fatty acid composition. *Journal of the American Oil Chemists' Society, 76*(5), 623–626.

Tian, C., Kasavajhala, K., Belfon, K. A. A., Raguette, L., Huang, H., Migues, A. N., Bickel, J., Wang, Y., Pincay, J., Wu, Q., & Simmerling, C. (2020). ff19SB: Amino-acid-specific protein backbone parameters trained against quantum mechanics energy surfaces in solution. *Journal of Chemical Theory and Computation, 16*(1), 528–552.

Van Der Spoel, D., Lindahl, E., Hess, B., Groenhof, G., Mark, A. E., & Berendsen, H. J. C. (2005). GROMACS: Fast, flexible, and free. *Journal of Computational Chemistry, 26*(16), 1701–1718.

Wang, J., Wolf, R. M., Caldwell, J. W., Kollman, P. A., & Case, D. A. (2004). Development and testing of a general amber force field. *Journal of Computational Chemistry, 25*(9), 1157–1174.

Wang, P.-P., Luo, Z.-G., Chun-Chen, Xiong-Fu, & Tamer, T. M (2020). Effects of octenyl succinic anhydride groups distribution on the storage and shear stability of Pickering emulsions formulated by modified rice starch. *Carbohydrate Polymers, 228*, Article 115389.

Wu, F., Deng, J., Hu, L., Zhang, Z., Jiang, H., Li, Y., Yi, Z., & Ngai, T. (2020). Investigation of the stability in Pickering emulsions preparation with commercial cosmetic ingredients. *Colloids and Surfaces A, 602*, Article 125082.

Wu, J., & Ma, G. H. (2016). Recent studies of Pickering emulsions: Particles make the difference. *Small (Weinheim an der Bergstrasse, Germany), 12*(34), 4633–4648.

Zhang, Y., Karimkhani, V., Makowski, B. T., Samaranayake, G., & Rowan, S. J. (2017). Nanoemulsions and nanolatexes stabilized by hydrophobically functionalized cellulose nanocrystals. *Macromolecules, 50*(16), 6032–6042.

Zhu, M., Huan, S., Liu, S., Li, Z., He, M., Yang, G., Liu, S., McClements, D. J., Rojas, O. J., & Bai, L. (2021). Recent development in food emulsion stabilized by plant-based cellulose nanoparticles. *Current Opinion in Colloid & Interface Science, 56*, Article 101512.